17th World Conference on Earthquake Engineering, 17WCEE

Sendai, Japan - September 13th to 18th 2020

PERFORMANCE OF A DEMONSTRATION EARTHQUAKE EARLY WARNING SYSTEM IN THE SICHUAN-YUNNAN BORDER REGION

C.Y. Peng[1], Q. Ma[2], P. Jiang[3], W.H. Huang[4], D.K. Yang[5], H.S. Peng[6], J.S. Yang[7]

[1] *Professor, Institute of Geophysics, China Earthquake Administration, Beijing, 100081, China, pengchaoyong@cea-igp.ac.cn*
[2] *Professor, Institute of Engineering Mechanics, China Earthquake Administration, Harbin 150080, China, maqiang@iem.ac.cn*
[3] *Engineer, Sichuan Earthquake Administration, Chengdu, 610041, China, jiang_0057@163.com*
[4] *Professor of Engineering, Shenzhen Academy of Disaster Prevention and Reduction, Shenzhen 518003, China, huangwh@163.com*
[5] *Professor, Institute of Geophysics, China Earthquake Administration, Beijing, 100081, China, yang.dake@qq.com*
[6] *Associate Professor, Department of Earthquake Monitoring and Prediction, China Earthquake Administration, Beijing 100036, China, penghs@cea.gov.cn*
[7] *Professor, Institute of Geophysics, China Earthquake Administration, Beijing, 100081, China, yangjiansi@vip.sina.com*

Abstract

Earthquake Early Warning Systems (EEWSs) are considered to be one of the most effective means for seismic risk mitigation, in terms of both losses and societal resilience, by releasing an alarm immediately after an earthquake occurs and before strong ground shaking arrives the target sites to be protected. To gain experience for the National System for Fast Seismic Intensity Report and Earthquake Early Warning project, we deployed a demonstration EEWS in the Sichuan-Yunnan border region with low-latency data transmission. It used a hybrid seismic network with micro-electro-mechanical system-based sensors and broad-band seismographs. In this study, we described the structure of this EEWS and analyzed its performance in the first two years from January 2017 to December 2018. During this test period, the EEWS detected and processed a total of 126 M_L 3.0+ earthquakes, with excellent epicentral location and magnitude estimation. The average location and magnitude estimation errors for the first alert were 4.2 ± 7.1 km and 0.2 ± 0.31, respectively. For the earthquakes that occurred inside and outside the hybrid network, the first alert was generated 13.4 ± 5.1 s and 26.3 ± 13.5 s after the origin time (OT), respectively. We analyzed the performance of the EEWS for the 31 October 2018 *M* 5.1 earthquake, because it was the largest event that occurred inside the hybrid network during the test period. The first alert was obtained at 7.5 s after the OT, with a magnitude error of 0.1 magnitude unit, a location error of about 1 km, and a depth error of 8 km. Finally, we discussed the main differences between the EEWS's estimates and the catalogs obtained by the China Earthquake Network Center, and proposed improvements to reduce the reporting time. This study demonstrated that we constructed a reliable, effective hybrid EEWS for the test region, which can provide sufficient support for the design of the National EEW project.

Keywords: earthquake early warning; MEMS-based sensor; real-time seismology; strong ground motion

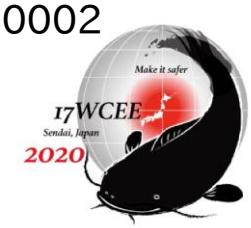

1. Introduction

Earthquake early warning (EEW) systems (EEWSs) aim at providing real-time estimates of earthquake parameters or expected ground-motion to the target sites soon after the occurrence of an earthquake and before these sites are struck by potentially damaging seismic waves. Presently, EEWSs have been developed or begun to be operated in various earthquake-prone countries and regions around the world, such as Japan [1], Mexico [2-4], Taiwan [5,6], California [7-9], Italy [10-12], and South Korea [13]. Operational EEWSs have shown great potentials by providing effective warnings for large earthquakes, like the 2011 M_w 9.0 Tohoku, Japan [14], the 2012 M_w 7.4 Oxaca, Mexico [15], the 2016 M_w 6.5 Meinong, Taiwan [16], the 2016 M_w 7.0 Kumamoto, Japan [17], and the 2018 M_w 6.2 Hualien, Taiwan, earthquakes [18,19]. These results gave local governments in other earthquake-prone countries enough confidence in establishing their own EEWSs.

In China, following the great 2008 Wenchuan earthquake, a group of seismologists recommended the government to build a nationwide EEWS, following examples in other countries with successful experiences. After several years of project proposal and feasibility studies, in June 2018, the National System for Fast Seismic Intensity Report and Earthquake Early Warning project, led by the China Earthquake Administration (CEA), was started, and the EEWS will be built in the next five years. Currently, the China Earthquake Network Center (CENC) is responsible for the design and implementation of this system. This nationwide EEWS will be mainly deployed in four key seismic zones, including the north-south seismic belt, Beijing capital region (BCR), northern Xinjiang area, and southeastern coastal areas. To cover the four key seismic zones with a high density of seismic stations and an average interstation distance of about 10-12 km, more than 10000 seismometers will be needed. Because of the high cost of traditional broad-band and force-balanced seismometers, the best way to lower the total investment of the project was to deploy a cost-effective seismic network by introducing low-cost micro-electro-mechanical system (MEMS)-based sensors [20]. On the basis of this design concept, the total investment of the project was reduced to 1.95 billion RMB, and when complete, the EEWS will comprise more than 15000 stations, containing 1928 seismic stations (equipped with co-located broad-band seismometers and force-balanced accelerometers), 3114 strong-motion stations (equipped with force-balanced accelerometers), and 10349 low-cost MEMS-based stations.

During the period of the project proposal, several prototype and demonstration EEWSs were created in parts of the four key seismic zones to explore and validate the scientific EEW feasibility. In this work, we focused on the demonstration EEWS deployed in the Sichuan-Yunnan border region and evaluated its real-time performance during the test period (2017-2018). We selected this area because, relative to the other eareas, more M_L 3.0+ earthquakes occurred in this region during the test period, including the 31 October 2018 M 5.1 Xichang, Sichuan, China, earthquake, which was the largest earthquake that occurred in the test regions since the first prototype EEWS was built up in the BCR. With the real-time processed results for these events, we were able to demonstrate the EEWS and provide a thorough evaluation for the National EEW project.

2. The demonstration EEW network

Since 2015, with the support of the CEA Department for Earthquake Monitoring and Prediction, the Sichuan Earthquake Administration (SEA) and the Yunnan Earthquake Administration (YEA) jointly constructed a hybrid demonstration EEWS. Following two years of installation work, 270 MEMS-based stations were deployed and configured, including 170 GL-P2B stations [20,21] and 100 Palert stations [5,6,19]. These two types of instruments have a low-latency data packetizing function that is designed specifically to support an EEWS. Compared with the Palert device, the GL-P2B device has a relatively high signal resolution because a high-dynamic range MEMS with about 100 dB was used in its development [20]. In addition, 13 local broad-band seismic stations were introduced into the system, in which only 3 stations in Yunnan were upgraded using the same low-latency data packetizing function and the other 10 stations in Sichuan still adopted the high-latency data transmission protocol with 512 bytes packet. Fig. 1 shows the station distribution of the hybrid demonstration EEW network. The SEA was responsible for building 150 GL-P2B

stations, including 40 stations co-located with traditional trigger-mode strong-motion stations, and the YEA deployed 100 Palert stations and 20 GL-P2B stations co-located with traditional trigger-mode strong-motion stations. In this system, we did not use the traditional trigger-mode strong-motion stations because the data recorded by these stations could not be transferred in real-time to the EEW processing center.

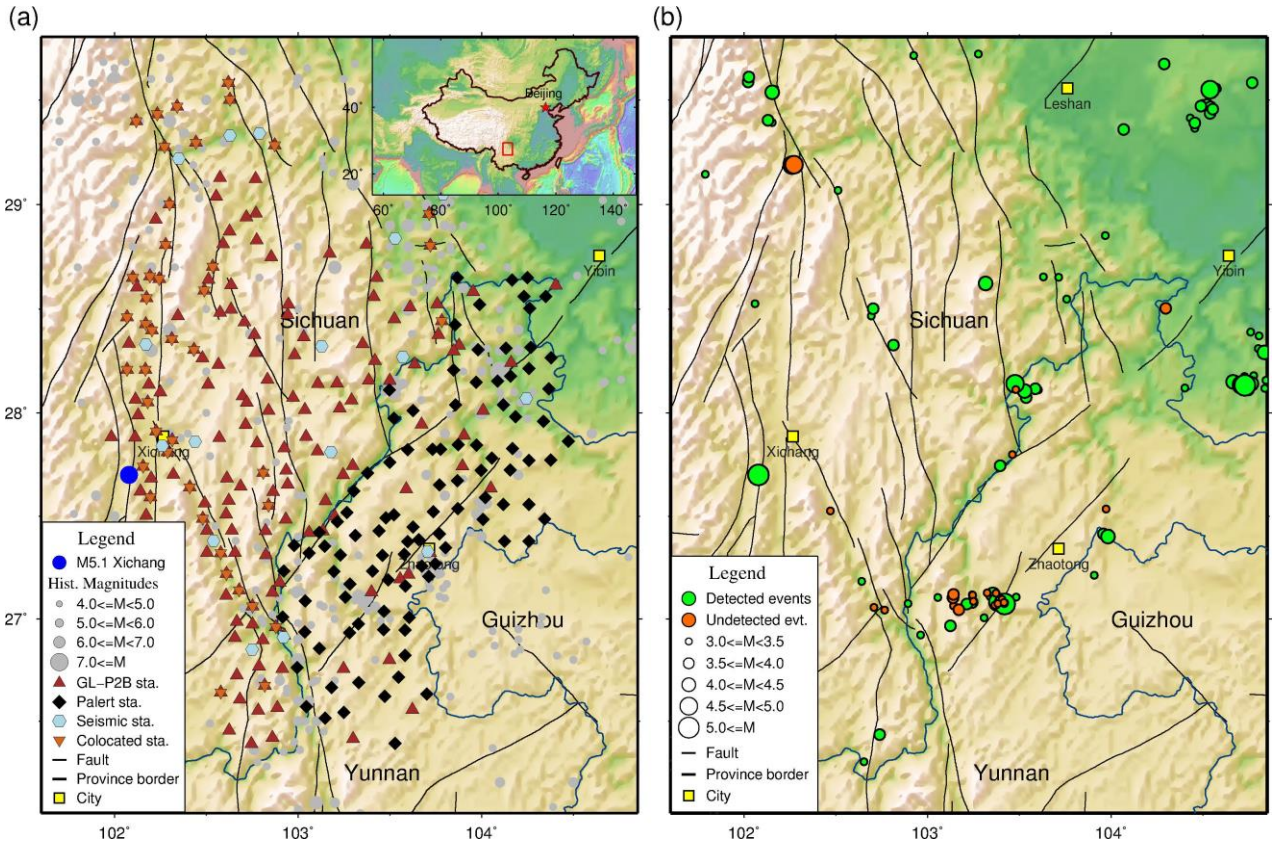

Fig. 1 – (a) Station distribution of the hybrid demonstration EEW network. The epicenters of historical earthquakes in this map were obtained from the U.S. Geological Survey catalog events and drawn as gray dots whose size is proportional to their magnitude. Brown triangles represent locations of the GL-P2B stations, in which some are co-located with traditional strong-motion stations (chocolate inverted triangles). Black diamonds show the locations of the Palert stations. The local seismic stations are plotted as light blue hexagons. The blue circle indicates the epicenter of the October 31, 2018, *M* 5.1 Xichang earthquake. A large map with marked studied region is shown in the inset. (b) Green and brown circles represent the events with M_L3.0 or more that were detected or undetected by the EEW system during the test period (2017-2018), with their size proportional to their magnitude. Black lines are faults reported by [22].

For the 60 GL-P2B sensors co-located with the traditional strong-motion stations (Fig. 2b), they used the same pier and power supply built for the traditional strong-motion stations. The other 110 GL-P2B stations were installed using a traditional station installation mode powered by 120 W solar panels and a 100 Ah backup battery (Fig. 2a). Most of the 100 Palert stations are located in elementary schools or at local government offices where power is provided (Fig. 2c). The real-time data recorded by the MEMS-based stations were transferred through 3G/4G mobile Internet signals to the Sichuan Earthquake Data Processing and Alert Issuing Center (Fig. 2d). All MEMS-based stations were operated at a sampling rate of 100 Hz and packetized with a maximum latency of 0.5 s. For the broad-band seismic stations, data recorded by 10 stations belonging to the SEA and 3 stations belonging to the YEA were acquired with data packetizing of 1 s and 0.2 s, respectively.

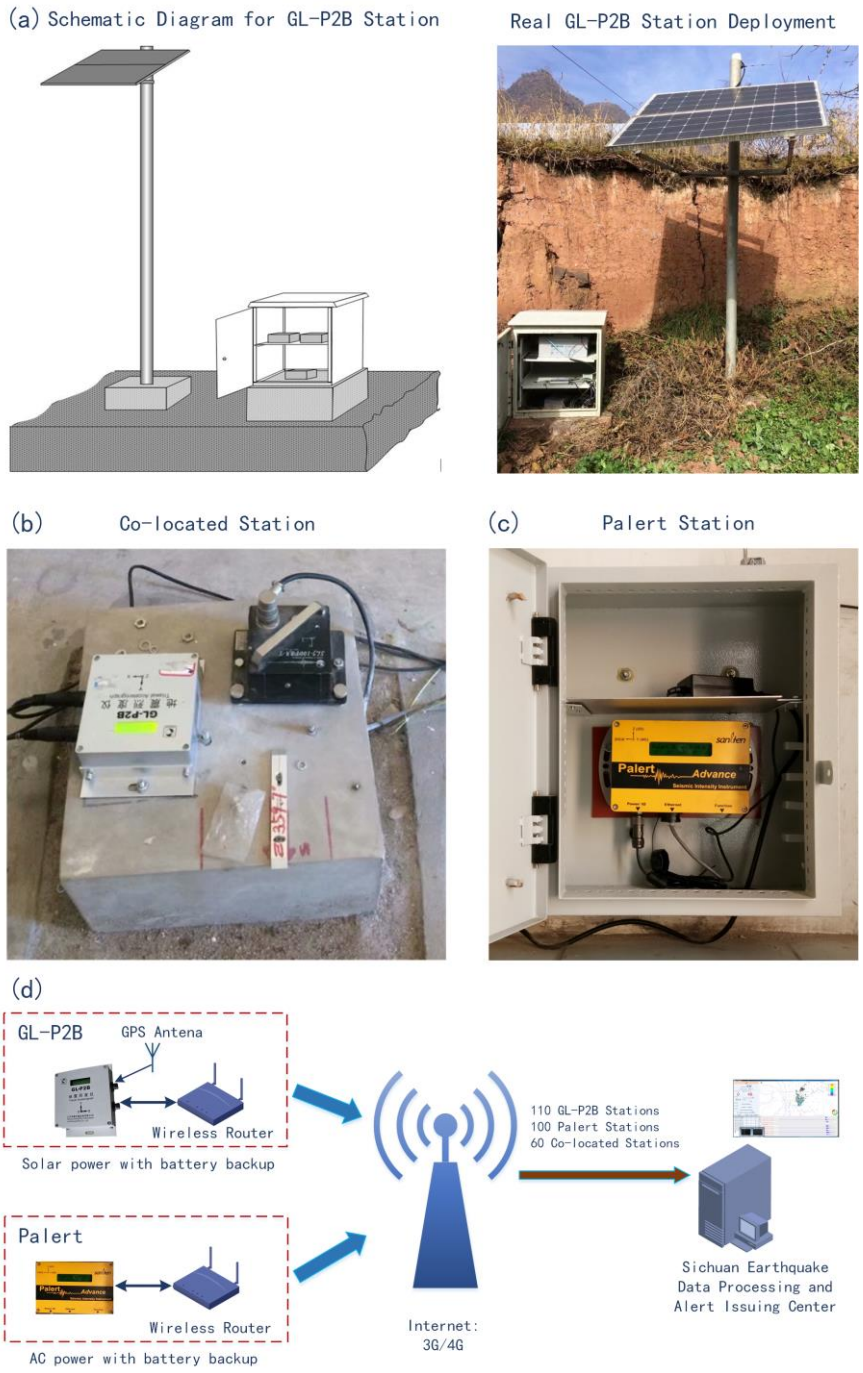

Fig. 2 – (a) Schematic diagram and photograph of the sensor installation for GL-P2B stations. (b) Photograph of one of the co-located stations with a force-balanced tri-axial accelerometer and an MEMS-based tri-axial accelerometer (GL-P2B). (c) Photograph of one of the Palert stations. (d) System structure for the hybrid demonstration EEW network.

2.1 EEW software structure

Fig. 3 shows the processing flow of the hybrid demonstration EEWS, which is a new version upgraded from that used in the first prototype EEWS [23]. This new version, written in Java, is designed specifically to maximize the hardware and software performance capabilities by improving both the speed and accuracy of the EEW processing. It includes a new seismic streaming server module. This module uses HTTP as the data

transmission protocol. To shorten the real-time data latency, it changed the data packetizing mode from the original 512 bytes to 256 bytes.

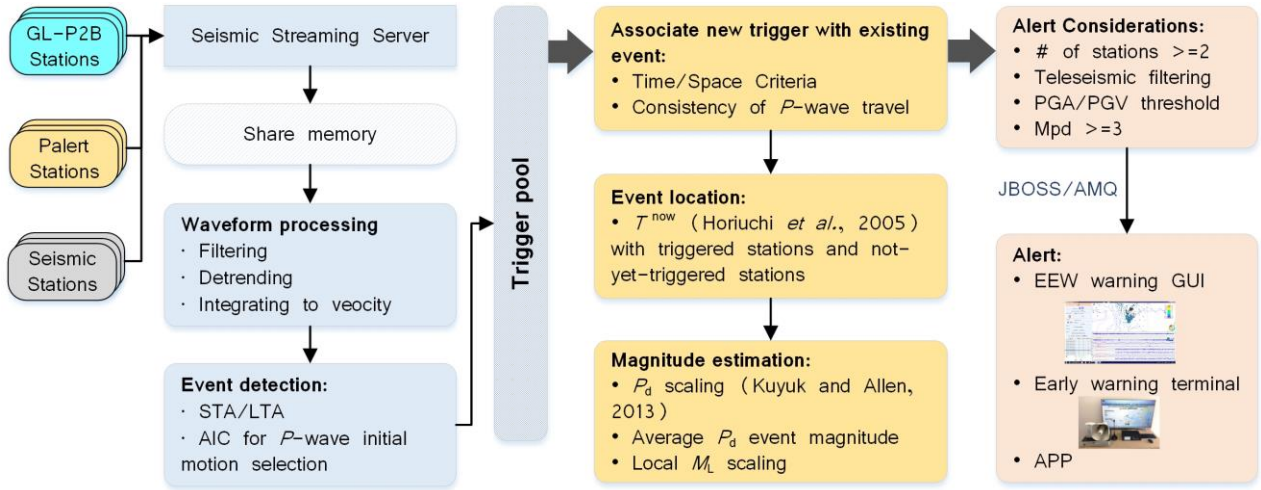

Fig. 3 – Processing flow for the hybrid demonstration EEWS.

We developed a real-time seismic phase picking module based on the short-term-average/long-term-average algorithm and Akaike information criterion to accurately detect the initial arrival of *P*-wave. These picks are then immediately forwarded to a trigger pool for event association. We use the T_{now} method [24] with triggered stations and not-yet-triggered stations for earthquake location and adopt the P_d scaling from [25] for EEW magnitude estimation. When *S*-wave is picked for the stations close to the earthquake epicenter (within 10 km), we directly use the local M_L scaling to compute the magnitude because the peak ground motion will arrive soon after the *S*-wave arrival, usually less than 1 or 2 s.

To reduce the rate of false alarms, we added several filters at the end of EEW processing and before an alert message is issued. First, the event must have been triggered by at least two stations. Second, we used a teleseismic filtering to discriminate between local and teleseismic events to avoid false alerts from large-magnitude teleseisms [7]. This filter is based on the different frequency content (τ_p^{max}) between the local and teleseismic events. Generally, waveforms from the teleseismic events tend to have longer-period content than the waveforms of the local earthquakes. In this work, we directly used the linear discriminant developed by [7] to separate local and teleseismic events. In addition, we applied different empirical peak ground motion thresholds to the initial portions of *P*-wave time windows according to the background noise level and device performance of different types of stations, such as 0.01 gal for seismic stations and 0.5 gal for MEMS-based stations. Furthermore, an event magnitude must be greater than 3. We continuously applied these alert filters to the associated events. Once an event met these criteria, it was issued immediately to the early-warning terminal. The event information could be updated when EEW parameters were refined with an enlarged *P*-wave time window or additional data from newly triggered stations.

3. System performance in the test period

Since January 2017, the implemented demonstration EEWS has operated using the hybrid network. According to the operational requirements, we needed to evaluate the average *P*-wave latencies of all stations in the network once per month. Here, the *P*-wave latency was the difference between the *P*-wave arrival at a station and the time when that trigger was detected by the EEWS. It included the time required for sensors and dataloggers to packetize the data and the telemetry latencies defined as the transmit time of data from the station to the processing module of the EEWS. The median *P*-wave latency for all stations in December 2018 was 0.89 ± 0.51 s (Fig. 4). The relatively large standard error was due to the large latencies introduced by the 10 seismic stations belonging to the SEA, because the dataloggers used in these stations

have not been upgraded for EEW purpose and still adopted the old data transmission protocol with 512 bytes packet. After excluding the values of these stations, the median *P*-wave latency was reduced to 0.81 ± 0.29 s. Detailed information for the *P*-wave latencies for each type of stations is listed in Table 1.

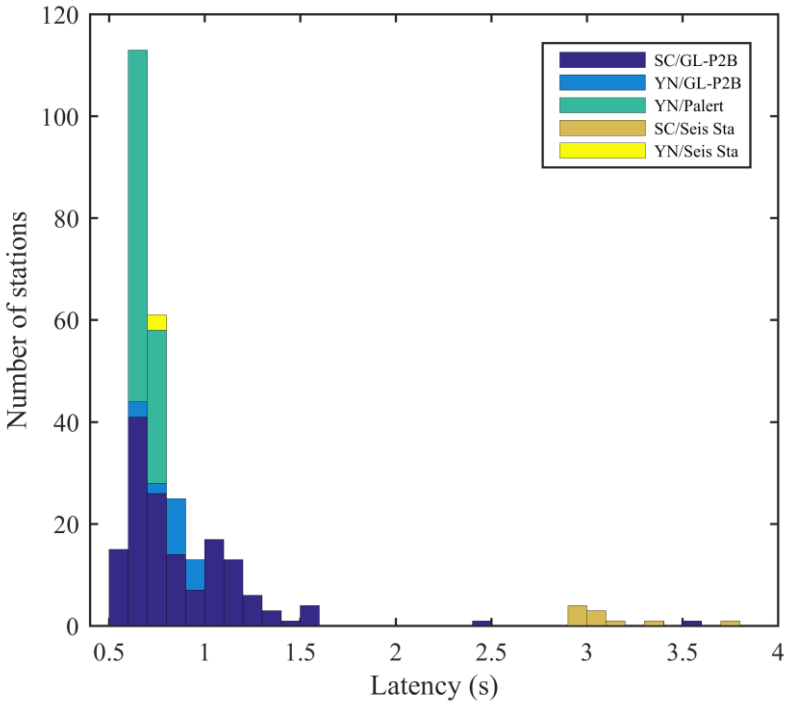

Fig. 4 – Latency historgram for the hybrid demonstration EEWS. GL-P2B stations deployed in Sichuan (SC/GL-P2B) and Yunnan (YN/GL-P2B) sent 0.5 s data packets; Palert stations deployed in Yunnan (YN/Palert) sent 0.5 s data packets; Seismic stations deployed in Sichuan (SC/Seis Sta) sent 1 s data packets; Seismic stations deployed in Yunnan (YN/Seis Sta) sent 0.2 s data packets.

Table .1 – Median *P*-wave latency for each type of stations

Station Type	Median (s)	S.D. (s)
All stations	0.89	0.51
SC/GL-P2B Stations	0.87	0.29
YN/GL-P2B Stations	0.85	0.11
YN/Palert Stations	0.69	0.02
SC/Seismic Stations	3.12	0.27
YN/Seismic Stations	0.77	0.01

During the test period from January 2017 to December 2018, approximately 175 earthquakes with M_L magnitude 3.0 or more occurred in or around the network, including 20 earthquakes with M_L 4.0 or more. To evaluate the performance of the demonstration EEWS, we selected the first alert to derive all statistics, because it is the most important for EEW. We compared each earthquake identified by the EEWS with those in the CENC catalogs, determined off-line and manually. We defined warning levels based on the catalog magnitude of an earthquake, that is, successful warning, false alarm, and missed warning. The threshold for a

warning was defined as magnitude 3.0. Following these definitions, for the 175 earthquakes, the EEWS successfully issued warnings for 126 earthquakes, missed 29 earthquakes inside the network and 20 outside the network. There were no false alarms issued during the test period. The main reasons can be attributed to the requirement of multiple station detections, the high acceleration threshold for *P*-wave declaration with low-cost sensors and the high density of the sensor network. Here, an earthquake inside the network represents that the distance of its epicenter to the nearest stations is less than 15 km. Otherwise, the earthquake is defined as an earthquake outside the network. In this study, we considered only the missed earthquakes that occurred inside the network. Results are summarized in Fig. 5.

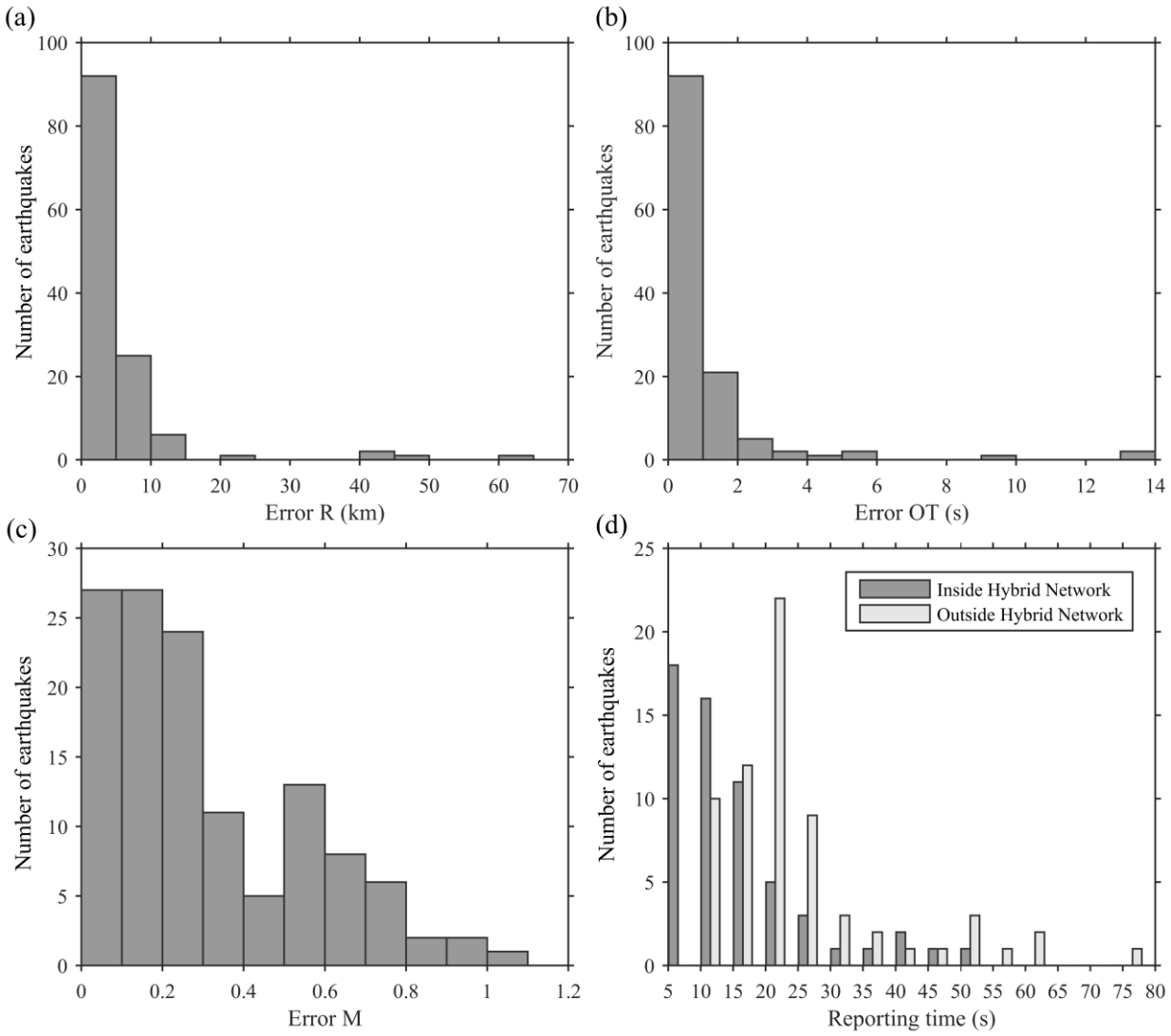

Fig. 5 – (a)-(c) Number of earthquakes versus differences between the first alert estimates output by the hybrid demonstration EEWS and catalogs obtained from the China Earthquake Network Center for epicenter, origin time, and magnitude. (d) Number of earthquakes as a function of the reporting time. Gray bars indicate earthquakes occurring inside the hybrid EEW network, and white bars are those occurring outside the network.

The epicentral error of the EEWS is shown in Fig. 5a. The average difference in epicenter location was 4.2 km, with a standard deviation of 7.1 km. Approximately 74% and 93% of the detected earthquakes had errors of less than 5 km and 10 km, respectively. Most of the earthquakes with epicentral errors of more than 10 km were located outside the network.

The estimated epicenter directly influenced the origin time (OT) estimated by the EEWS, and therefore those earthquakes with large errors in epicenter estimation also had a large error in the OT (Fig. 5a, b). The average difference in OT was 1.1 s with a standard deviation of 2.0 s, and approximately 74% of the detected earthquakes had an error of less than 1 s. The greatest difference was about 13.6 s for two earthquakes located outside the network. The reason for those earthquakes with large OT errors was the same as those with epicentral errors of more than 10 km.

Fig. 5c shows the error in *M*. Most of the earthquakes had an error of less than 0.6 (85%), including 62% with an error of no more than 0.2. The average difference in magnitude estimation was 0.2 ± 0.31, in which the positive 0.2 value indicated that, on average, the EEWS slightly overestimated the magnitude by 0.2 magnitude units. This may be attributed to the high-background noise levels of the deployment sites and the relatively low resolution of the MEMS-based sensors. For only the larger events ($M_L \geq 4.0$), the errors were -0.1 ± 0.24.

Another important characteristic that had to be evaluated for an EEWS was reporting time, which is defined as the time needed to issue the alert after the OT. For the two years of the hybrid network's operation, the average reporting time for earthquakes occurring inside the network was 13.4 ± 5.1 s (Fig. 5d). Fig. 5d shows that for earthquakes occurring inside the network, the shortest reporting time was 6 s after the OT and the longest was 53 s. For the majority of events, the reporting time was less than 20 s, indicating that the EEWS could issue an EEW report within approximately 20 s after an earthquake occurred. For earthquakes outside the network, the fastest reporting time was 11 s and the longest was 78 s, with a mean warning time of 26.3 s and a standard deviation of 13.5 s.

4. Performance for the 2018 *M* 5.1 Xichang earthquake

During the test period, an *M* 5.1 earthquake with a depth of 19 km occurred on October 31, 2018, in Mopan (27.7° N, 102.08° E), Sichuan province, China (Fig. 1), about 28 km from Xichang City. Thus far, this event was the largest earthquake occurring within the test regions that was detected since the first prototype EEW system was built in the BCR. The first warning was issued 7.5 s after the OT. Fig. 6 presents the real-time responses of the EEWS for this earthquake. Approximately 6.5 s after the OT, the EEWS created the event and obtained the first result. Because the estimated magnitude did not reach the threshold, this result was not issued. After 1 s, the EEWS immediately issued the first warning when the thresholds for the magnitude and the number of triggered stations were satisfied.

The EEWS estimated an *M* 5.1 at the first warning, which was consistent with the magnitude calculated by the CENC (Fig. 6b). By progressively expanding the *P*-wave time windows and including more triggered stations, the estimated magnitude had only a small variation until it reached the final estimated value of 5.0. The epicentral location was the best determined parameter. The first result was similar to that of the CENC (Fig. 6c), with a difference of about 1 km. Because most of the triggered stations were located on the right side of the earthquake epicenter, this led to a slightly large error in longitude when we used more triggered stations to estimate the epicenter parameter. The depth estimation exhibited a relatively large variation (Fig. 6d). The estimated value first increased and then decrease until it reached its final result of 12 km, representing an error of 7 km relative to the depth estimated by the CENC (19 km).

This earthquake was felt widely over the study area, with the highest intensity of VI at more than 10 towns of Xichang City (http://www.scdzj.gov.cn/xwzx/fzjzyw/201811/t20181102_49990.html). Considering an S-wave velocity of 3.5 km/s, this event has a blind zone with radii of about 19 km around the epicenter. Xichang City had a 2 s lead time, which increased to 11 s for the Xichang Satellite Launch Centre (61 km from the epicenter). The lead time is defined as the interval between the time when the first warning is issued and the time PGA is recorded.

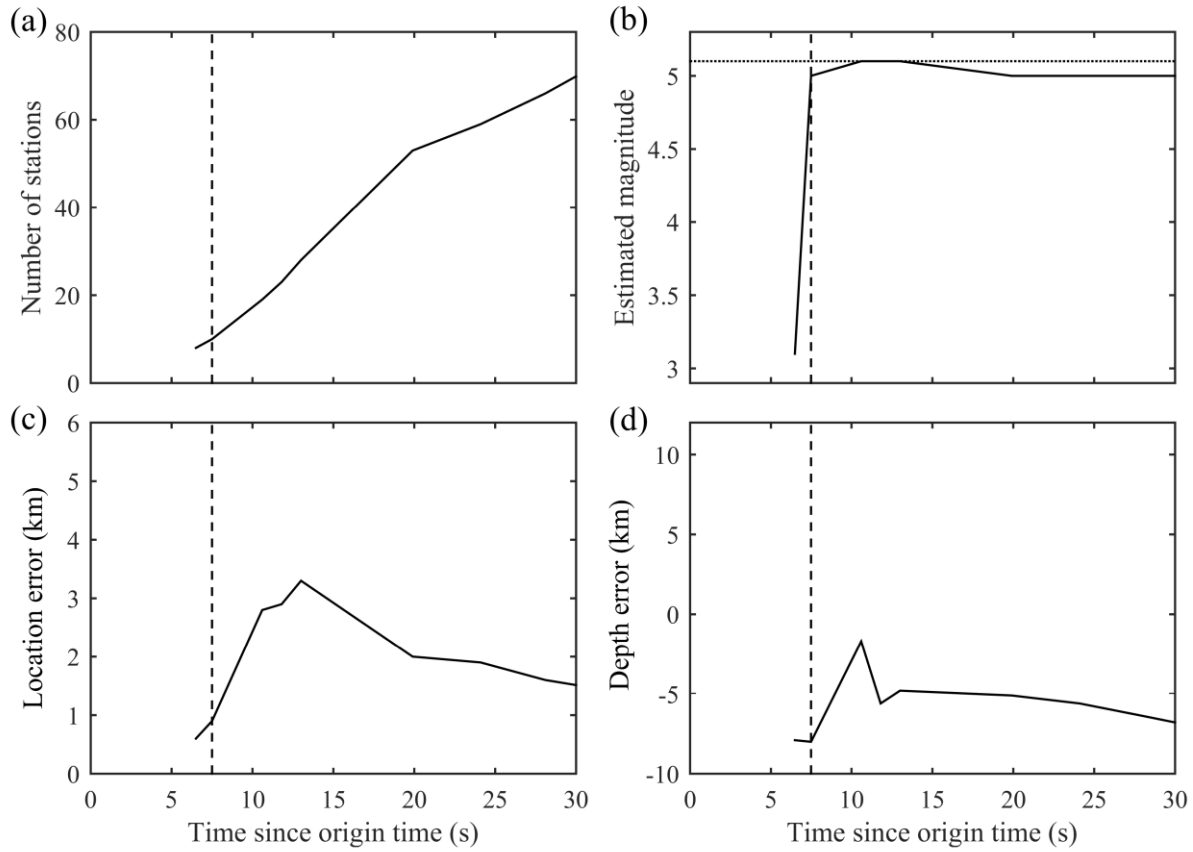

Fig. 6 – Real-time response of the hybrid demonstration EEWS for the *M* 5.1 earthquake on October 31, 2018: (a) number of triggered stations, (b) magnitude error, (c) location error, and (d) depth error as a function of time since the earthquake occurred. Vertical dashed lines represent the first alert time, and the horizontal dotted line indicates the catalog magnitude *M* 5.1 of the Xichang earthquake.

5. Discussion and conclusion

The hybrid EEWS began delivering EEW information in January 2017. The software used in this system was an updated version of the first prototype EEW installed in the BCR. With algorithm optimization in magnitude estimation and earthquake detection, introduction of low-latency data transmission, and inclusion of more stations, performance of the EEWS was significantly improved. During the test period, the EEWS issued 126 warnings for earthquakes with magnitude no less than M_L 3.0 occurring in the study region. The OT and epicenter were the two best determined parameters, with differences of less than 2 s and 10 km for most cases (90% and 93%) regardless of whether the earthquake occurred inside or outside the hybrid EEW network. As to the magnitude, about 85% of the earthquakes had an error of no more than 0.5, which was most notable for the Xichang *M* 5.1 earthquake with a magnitude error of 0.1.

Inside the hybrid network, however, 29 earthquakes with M_L 3.0 or more were not detected by the EEWS (Figs. 1b), in which only one event's magnitude (M_L 4.9) was larger than 4.0. Most of these missed earthquakes occurred in the Yunnan region monitored by the Palert-based stations. We attributed these missed earthquakes to the low signal resolution (16 bits) of the Palert device, which is more suitable for earthquakes with a magnitude greater than 4.0 [5, 26]. The M_L 4.9 earthquake occurred 29 s after a previous event with M_L 4.6 at the same location. This time was within the event detection threshold of 49 s used to avoid considering the secondary arrivals at the same station as a new earthquake. Because reducing this threshold would be controversial and could lead to false alarms, this problem should be considered as an

inherent limitation of the current EEWS [27]. To reduce the influences of this limitation on the EEWS, we can introduce some effective algorithms like the integrated particle filter and propagation of local undamped motion methods to process multiple simultaneous earthquakes within a short distance [17].

Lead time strongly influenced the usefulness of an EEWS, which depended on the time needed to report the warning and the epicenter distance of the target site. The average reporting times for an earthquake inside and outside the hybrid network were 13.4 s and 26.3 s, respectively (Fig. 5d). This indicated that the system can offer warning information to regions with an epicentral distance greater than 45 km for earthquake inside the network. This result was comparable to that of the Palert system deployed in Taiwan [5, 26]. However, if we only focused on the M_L 4.0+ events, the average reporting time were reduced to 9.34 ± 1.22 s because of relatively high signal-to-noise ratio of each station recording. The reporting time was further reduced to 7.5 s for the M 5.1 Xichang earthquake with about 19 km blind zone around the epicenter. Currently, this was one of the best results obtained by the EEWS for an earthquake. To further reduce the reporting time, we could take additional measures, such as improving the 3G/4G network environment by moving the MEMS-based stations to the mobile base stations or optimizing the currently adopted algorithms by calibrating new relationships with the data collected in this system. We also could shorten the reporting time by introducing an onsite warning algorithm based on the $P_d/P_v/P_a$ or PGA thresholds [28, 29], like those adopted in the Palert system [5, 26] or the stand-alone EEWS [12] or the NEEWS [16, 18]. Additionally, these onsite warning algorithms could work as a backup method that detects and reports strong motions from large events occurred immediately after a small earthquake within a short distance or at the same location.

Another limitation in this work is that the proposed system employs a simple point-source algorithm that calculates magnitudes based on P_d. This will lead to underprediction of ground motions for large (M~7 or more) earthquakes because of magnitude saturation and no consideration of fault finiteness. We can effectively solve this limitation by introducing real-time finite-source estimation algorithms (e.g. [30-33]) into our system.

From this work, with the current configuration of the hybrid EEW network in the Sichuan-Yunnan border region, the demonstration EEWS provided reliable earthquake warnings for the test region. With establishment of a nationwide EEW system in the near future, this system can provide sufficient support for the design of this huge project.

6. Acknowledgements

All data used in this study, including the broad-band seismic waveforms and the MEMS-based recordings, were obtained from the Sichuan Earthquake Administration (http://www.scdzj.gov.cn). For information about access to the data for research purposes, please contact jiang_0057@163.com. The earthquake catalogs used for compared with the results of hybrid demonstration EEWS were derived from the China Earthquake Network Center (CENC; http://news.ceic.ac.cn, last accessed March 2019). This research was supported by National Key R&D Program of China (Grant no. 2018YFC1503904) and Beijing Natural Science Foundation (8202051). The GMT software from [34] was used in plotting part of the figures and is gratefully acknowledged.

7. References

[1] Hoshiba M, Kamigaichi O, Saito M, Tsukada S, Hamada N (2008): Earthquake early warning starts nationwide in Japan. *Eos Transactions AGU*, **89**(8), 73-74.

[2] Espinosa-Aranda JM, Cuéllar A, García A, Ibarrola G, IsIas R, Maldonado S, Rodriguez FH (2009): Evolution of the Mexican Seismic Alert System (SASMEX). *Seismological Research Letters*, **80**, 694-706.

[3] Cuéllar A, Suárez G, Espinosa-Aranda JM (2017): Performance evaluation of the earthquake detection and classification algorithm 2(t_S–t_P) of the Seismic Alert System of Mexico (SASMEX). *Bulletin of the Seismological Society of America*, **107**(3), 1451-1463.

[4] Suárez g, Espinosa-Aranda JM, Cuéllar A, Ibarrola G, García A, Zavala M, Maldonado S, Islas R (2018): A dedicated seismic early warning network: The Mexican Seismic Alert System (SASMEX). *Seismological Research Letters*, **89**(2A), 382-391.

[5] Wu YM (2014): Progress on development of an earthquake early warning system using low-cost sensors. *Pure and Applied Geophysics*, **172**(9), 2343-2351.

[6] Wu YM, Liang WT, Mittal H, Chao WA, Lin CH, Huang BS, Lin CM (2016): Performance of a low-cost earthquake early warning system (P-alert) during the 2016 ML 6.4 Meinong (Taiwan) earthquake. *Seismological Research Letters*, **87**(5), 1050-1059.

[7] Kuyuk HS, Allen RM, Brown H, Hellweg M, Henson I, Deuhauser D (2014): Designing a network-based earthquake early warning algorithm for California: Elarms-2. *Bulletin of the Seismological Society of America*, **104**, 162-173.

[8] Kohler MD, Cochran ES, Given D, Guiwits S, Neuhauser D, Henson I, Hartog R, Bodin P, Kress V, Thompson S, Felizardo C, Brody J, Bhadha R, Schwarz S (2018): Earthquake early warning ShakeAlert system: west coast wide production prototype. *Seismological Research Letters*, **89**(1), 99-107.

[9] Chung AI, Henson I, Allen RM (2019): Optimizing earthquake early warning performance: ElarmS-3. *Seismological Research Letters*, **90**(2A), 747-743.

[10] Zollo A, Amoroso O, Lancieri M, Wu YM, Kanamori H (2010): A threshold-based earthquake early warning using dense accelerometer networks. *Geophysical Journal International*, **183**, 963-974.

[11] Satriano C, Elia L, Martino C, Lancieri M, Zollo A, Iannaccone G (2011): PRESTo, the earthquake early warning system for southern Italy: concepts, capabilities and future perspectives. *Soil Dynamics and Earthquake Engineering*, **31**, 137-153.

[12] Festa G, Picozzi M, Caruso A, Colombelli S, Cattaneo M, Chiaraluce L, Elia L, Martino C, Marzorati S, Supino M, Zollo A (2018): Performance of earthquake early warning systems during the 2016-2017 M_w 5-6.5 central Italy sequence. *Seismological Research Letters*, **89**(1), 1-12.

[13] Sheen DH, Park JH, Chi HC, Hwang EH, Lim IS, Seong YJ, Park J (2017): The first stage of an earthquake early warning system in South Korea. *Seismological Research Letters*, **88**(6), 1491-1498.

[14] Fujinawa Y, Noda Y (2013): Japan's earthquake early warning system on 11 March 2011: performance, shortcomings, and changes. *Earthquake Spectra*, **29**(s1), S341-S368.

[15] Cuéllar A, Espinosa-Aranda JM, Suárez G, Ibarrola G, Uribe A, Rodríguez FH, Islas R, Rodríguez GM, García a, Frontana B (2014): The Mexican Seismic Alert System (SASMEX): its alert signals, broadcast results and performance during the *M* 7.4 Punta Maldonado earthquake of March 20th, 2012, in Wenzel F, Zschau J (eds), *Early Warning for Geological Disasters*, 71-87, Springer, Berlin, Heidelberg.

[16] Hsu TY, Wang HH, Lin PY, Lin CM, Kuo CH, Wen KL (2016): Performance of the NCREE's on-site warning system during the 5 February 2016 M_w 6.53 Meinong earthquake. *Geophysical Research Letters*, **43**, 8954-8959.

[17] Kodera Y, Saitou J, Hayashimoto N, Adachi S, Morimoto M, Nishimae Y, Hoshiba M (2016): Earthquake early warning for the 2016 Kumamoto earthquake: performance evaluation of the current system and the next-generation methods of the Japan Meteorological Agency. *Earth Planets Space*, **68**, 202, doi:10.1186/s40623-016-0567-1.

[18] Hsu TY, Lin PY, Wang HH, Chiang HW, Chang YW, Kuo CH, Lin CM, Wen KL (2018): Comparing the performance of the NEEWS earthquake early warning system against the CWB system during the 6 February 2018 M_w 6.2 Hualien earthquake. *Geophysical Research Letters*, **45**, 6001-6007.

[19] Wu YM, Mittal H, Huang TC, Yang BM, Jan JC, Chen SK (2019): Performance of a low-cost earthquake early warning system (P-alert) and shake map production during the 2018 M_w 6.4 Hualien, Taiwan, earthquake. *Seismological Research Letters*, **90**(1), 19-29.

[20] Peng CY, Chen Y, Chen QS, Yang JS, Wang HT, Zhu XY, Xu ZQ, Zheng Y (2017): A new type of tri-axial accelerometers with high dynamic range MEMS for earthquake early warning. *Computers & Geosciences*, **100**, 179-187.

[21] Peng CY, Jiang P, Cheng QS, Ma Q, Yang JS (2019): Performance evaluation of a dense MEMS-based seismic sensor array deployed in the Sichuan-Yunnan border region for earthquake early warning. *Micromachines*, **10**, 735.

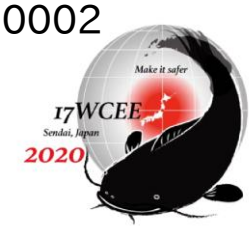

[22] Deng QD, Zhang PZ, Ran YK, Yang XP, Min W, Chu QZ (2003): Basic characteristics of active tectonics of China. *Science in China Series D: Earth Sciences*, **46**(4), 356-372.

[23] Peng HS, Wu ZL, Wu YM, Yu SM, Zhang DN, Huang WH (2011): Developing a prototype earthquake early warning system in the Beijing Capital Region. *Seismological Research Letters*, **82**(3), 394-403.

[24] Horiuchi S, Negishi H, Abe K, Kamimura A, Fujinawa Y (2005): An automatic processing system for broadcasting earthquake alarms. *Bulletin of the Seismological Society of America*, **95**, 708-718.

[25] Kuyuk HS, Allen RM (2013): A global approach to provide magnitude estimates for earthquake early warning alerts. *Geophysical Research Letters*, **40**, 6329-6333.

[26] Wu YM, Chen DY, Lin TL, Hsieh CY, Chin TL, Chang WY, Li WS, Ker SH (2013): A high-density seismic network for earthquake early warning in Taiwan based on low cost sensors. *Seismological Research Letters*, **84**(6), 1048-1054.

[27] Carranza M, Buforn E, Zollo A (2017): Performance of a network-based earthquake early warning system in the Ibero-Maghrebian region. *Seismological Research Letters*, **88**(6), 1499-1507.

[28] Peng CY, Yang JS, Zheng Y, Zhu XY, Xu ZQ, Chen Y (2017): New τ_c regression relationship derived from all *P* wave time windows for rapid magnitude estimation. *Geophysical Research Letters*, **44**, 1724-1731.

[29] Peng CY, Yang JS (2019): Real-time estimation of potentially damaged zone for earthquake early warning based on thresholds of *P*-wave parameters. *Acta Seismologica Sinica*, **41**(3), 354-365 (in Chinese).

[30] Yamada M, Heaton TH, Beck J (2007): Real-time estimation of fault rupture extent using near-source versus far-source classification. *Bulletin of the Seismological Society of America*, **97**(6), 1890-1910.

[31] Böse M, Heaton TH, Hauksson E (2012): Real-time Finite Fault Rupture Detector (FinDer) for large earthquakes. *Geophysical Journal International*, **191**, 803-812.

[32] Böse M, Smith DE, Felizardo C, Meier MA, Heaton TH, Clinton JF (2018): FinDer v.2: Improved real-time ground-motion predictions for M2-M9 with seismic finite-source characterization. *Geophysical Journal International*, **212**, 725-742.

[33] Crowell BW, Schmidt DA, Bodin P, Vidale JE, Gomberg J, Hartog JR, Kress VC, Melbourne TI, Santillan M, Minson SE, Jamison DG (2016): Demonstration of the Cascadia G-FAST geodetic earthquake early warning system for the Nisqually, Washington, earthquake. *Seismological Research Letters*, **87**(4), 930-943.

[34] Wessel P, Smith WHF (1998): New improved version of Generic Mapping Tools released. *Eos Transactions AGU*, **79**(47), 579, doi:10.1029/98EO00426.

